

Design and Adaptive Control of Matrix Transformer Based Indirect Converter for Large-Capacity Circuit Breaker Testing Application

Liang Shu , Member, IEEE, Ziran Wu , Yingmin You, Marcelo J. Dapino , and Sheng Zhao

Abstract—Circuit breakers (CBs) play an important role in distribution networks. According to IEC standards, protection characteristics need to be investigated to ensure reliability in the manufacturing process. It is required from IEC 60947 that the instantaneous release shall be verified with a test current at least 10 times greater than the rated current. For large-capacity CB testing, converters with large output current, high accuracy and fast response are needed. A large current indirect converter including four converting units and a matrix transformer is proposed. The converting units are synchronized using a complex programmable logic device (CPLD)-based logic control unit. To increase the current accuracy, an adaptive feedforward control strategy is developed to compensate for the influences of CB-dependent resistances and inductances. The equivalent load impedance is adaptively identified from a robust identifier, which is then used to construct the feedforward compensator. Simulation and experimental results show that different CBs create CB-dependent contact resistances and inductances in the testing circuit. The impedance change can be successfully identified by the robust identifier with limited errors. The proposed converter is capable of generating a wide range of current from 100 A to 40 kA with an error no greater than 2.2%.

Index Terms—Circuit breaker (CB) testing, impedance identification, indirect converter, robust adaptive control.

I. Introduction

IRCUIT breakers (CBs) are mainly designed to interrupt current flow when faults are detected, and have been

Manuscript received June 25, 2019; revised October 12, 2019, December 25, 2019, and March 18, 2020; accepted April 5, 2020. Date of publication April 21, 2020; date of current version February 17, 2021. This work was supported in part by the National Natural Science Foundation of China under Grant 51975418, in part by the Key Technology Project of Wenzhou under Grant 2018ZG020, and in part by the Zhejiang Technology Research Plan under Grant LGC20E070001. (Corresponding author: Ziran Wu.)

Liang Shu, Ziran Wu, Yingmin You, and Sheng Zhao are with the Key Laboratory of Low-Voltage Apparatus Intellectual Technology of Zhejiang, Wenzhou University, Wenzhou 325027, China (e-mail: liang.shu9@gmail.com; nature.nano@gmail.com; yymfd@qq.com; zs_sea501@wzu.edu.cn).

Marcelo J. Dapino is with the Department of Mechanical and Aerospace Engineering, The Ohio State University, Columbus, OH 43210 USA (e-mail: dapino.1@osu.edu).

Color versions of one or more of the figures in this article are available online at https://ieeexplore.ieee.org.

Digital Object Identifier 10.1109/TIE.2020.2988191

widely used in industrial applications [1], [2]. According to IEC standards (IEC 60898 [3], IEC 60947 [4]), the protection characteristics need to be tested when the circuits encounter different fault currents (over-load, short-circuit, etc.). It is required in IEC standards that the accuracy of the CB testing instrument is within 5%. To develop high precision testing tools that can also provide online quality inspection, it is important to improve product quality and manufacturing efficiency. High precision current conversion with tunable magnitude is an effective way to implement the tests [5]–[9]. Based on the topology design, current converters can be typically divided into direct ac-ac converters [5]-[7], indirect ac-dc-ac converters [8]-[10] and matrix converters [11], [12]. Research work was reported in [5] that a single phase ac-ac converter was developed to verify the protection characteristics of miniature circuit breakers (MCBs) with rated current (I_n) less than 125 A. An AC-ac converter with controllable phase and amplitude was discussed in [6] by adopting the concept of virtual quadrature source. A maximum current of 750 A was tested. To increase current accuracy, an improved single phase direct pulsewidth modulation (PWM) inverting ac-ac converter was developed in [7] to solve the shoot-through and dead-time problems. Applications of indirect converters were discussed in [8]-[10]. With the existence of a dc link capacitor, the indirect converter is capable of providing both variable output voltage and variable frequency. Also, since both the dc capacitor voltage and the inverting voltage can be controlled, implementation of a closed loop controller is easier. The matrix converters can be developed from their direct ac-ac counterparts by adding additional active switches [11]. With the added bidirectional phase legs, the matrix converter can provide variable output voltage and frequency with directly connected input power supply to load without an intermediate dc-link capacitor. However, this increases the system cost and the control complexity. Also, these methods are only capable of generating controllable currents with limited magnitudes, which means they are only suitable for small size CB test, e.g., MCBs.

Requirements of CBs testing are stated in two IEC standards, IEC 60898 (rated current less than 125 A) and IEC 60947 (rated current larger than 125 A). To implement the tests for breakers with rated current larger than 125 A (defined as large capacity CB), IEC 60947 specifies that the connected voltage

0278-0046 © 2020 IEEE. Personal use is permitted, but republication/redistribution requires IEEE permission. See https://www.ieee.org/publications/rights/index.html for more information.

be rated voltage not to exceed 1000 V ac or 1500 V dc, and the instantaneous release shall be verified with a test current at least 10 times greater the rated current. For example, to test an ACB (air circuit breaker), the testing current usually needs to go up to 40 kA, which exceeds the output limit of the aforementioned designs. There are two main challenges to develop such testing instruments, first, the very high current generation topology and second, the corresponding control strategy to ensure high current accuracy. To increase the current ratings, several methods have been discussed. In [5] and [13], it was introduced that commercially available current sources for CB testing were based on the motor-driven auto-transformer design. The transformer tap was connected with a digital motor and the testing current could be generated by controlling the motor position. However, the accuracy of this method is not guaranteed. Also, since the current needs to be controlled via tuning of the motor's motion, the efficiency is severely limited.

Another method to generate large current is to construct parallel power switches [14]-[18]. A paralleled insulated gate bipolar transistor (IGBT) module with rated current of 3000 A was studied in [14] to be used in a 2 MW wind turbine system. In [15], an active gate control for balancing the currents in paralleled IGBT modules was presented. It was shown that 20 kA pulses (5 kA per IGBT) were obtained with errors within 5%. Another method to reduce the unbalanced current of paralleled IGBTs was discussed in [16] and [17]. It was shown that six phase legs were operated in parallel to achieve the 3600 A rms inverter current. Application of paralleled thyristors was discussed in [18]. A 35 kA thyristor dc switch which consisted of eight paralleled thyristors was developed to meet the high current requirement. Paralleled power switches are helpful to generate large currents. However, parallel operation of power switches may result in huge circulating current and short circuit because of different time delays and parameter tolerances. The speed differences among switches may also lead to converting failure. Moreover, unbalanced local temperature rise is another challenge in the design.

We aim to develop an easily controlled high current converter with high accuracy and fast response for large-capacity CB testing applications. It is required that the converter be capable of generating both step current and ramped current with specified accuracy and speed. There are two different features for large-capacity CB testing. First, the impedance of the load is unknown in each test. The contact resistance and the inductance of the electromagnetic coil are unable to be determined before tests. Second, the load impedances are object-dependent (CB-dependent). Different CBs demonstrate different contact resistances and inductances. To guarantee current accuracy, control design that considers the influence of CB-dependent impedances needs to be developed.

Different methods have been discussed in the converter controller designs, including proportional integral (PI) control [5], [20], predictive control [12], [21], sliding mode control [22], sensorless control [23], [24], etc. A PI controller was used in [5] to maintain the dc-link voltage of an ac—ac converter for CB testing applications. Similar methods are used for voltage regulation in the power transmission system [20]. The PI structure is simple and can be easily implemented. However, the

dynamic response of this design is limited. To improve controller performance, predictive control was used in [12] and [21] to increase the dynamic responses. However, the performance of this method relies on the model's accuracy. If the model fails to reflect the physical dynamics of the plant, imprecision even instability could be induced. Sliding mode control is another method used for converter regulation. It is a variable structure control method, which allows the controller to handle system deviations. By constructing the sliding surface and the nonlinear switching term, the reference input can be correctly tracked provided the system deviation bounds are known [22]. However, determination of these bounds is usually very difficult [25]. Moreover, the fast switching frequencies will further increase the operation burden for power switches. Sensorless control that requires no current sensors is another method that was developed for cost-savings purposes. The feedback current is usually estimated from the input voltage [26] or the generated PWM signals [27]. The accuracy can be guaranteed if the electric load is fixed. However, for large-capacity CB testing, the contact resistances and inductances are CB-dependent and the accuracy is difficult to be guaranteed.

In this article, we have developed an easily controlled high current converter based on the matrix transformer design. The converter includes four paralleled converting units, which are synchronized by a CPLD-based logic control unit. A robust adaptive feedforward (RAF) control strategy is developed to compensate the influences of CB-dependent resistances and inductances. The proposed converter is capable of generating a wide range of currents from 100 A to 40 kA according to different requirements of large capacity CB testing.

II. PROPOSED SYSTEM

Large-capacity CBs need to provide three-zone protections in power distribution network, which is different from small size CBs. It is seen from Fig. 1 that large capacity CBs (QF1) are usually located on the supply side (close to the power supply) and the small size CBs (QF2) are located on the load side (close to the consumer) [19]. To ensure high power supply reliability, QF1 are designed with the function of three-zone protection, over load, delayed short-circuit and short-circuit. When a fault current $i_{\rm fault}$ arises at branch C, it is seen from Fig. 1(b) that QF2_c trips in advance of QF1, due to the function of delayed short-circuit protection (Zone 2). This special design ensures the reliability of the power supply for fault-free branches (Branch A and Branch B in Fig. 1).

To investigate the three-zone protection, IEC 60947 requires that the CB characteristics be tested under three different conditions, short circuit, overload, and definite time delay. Here, we only discuss the first two types (see Table I), since the third type is usually examined by the manufacturer. The testing procedure is illustrated in Table I. The testing currents should be generated according to different setting currents I_i , I_s , and I_r . Usually I_i is set as $5{\sim}10$ times of the rated current I_n , I_s is set as $3{\sim}5$ times of I_n , and I_r is $0.7{\sim}1.0$ times of I_n . Also, it is noted that the " $1.05I_r$ " and " $1.3I_r$ " tests should be conducted in sequence, which means there should be a step change in the continuous testing current generation.

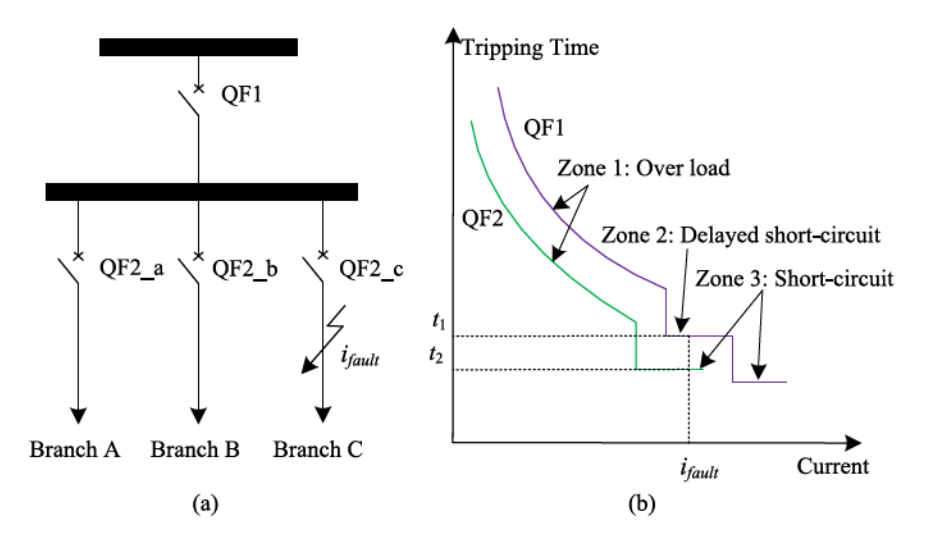


Fig. 1. Topology of power distribution network with different type of CBs.

TABLE I
TESTING REQUIREMENTS OF LARGE CAPACITY CBS

Types	Testing current	Tripping limits and characteristics
Type I	$80\%I_i$	No tripping for 0.2 s, or a time interval equal to twice the time-delay stated by the manufacturer.
	$120\%I_i$	Tripping within 0.2 s, or a time interval equal to twice the time-delay stated by the manufacturer.
Type II	90 %I _s	No tripping for 0.2 s, or a time interval equal to twice the time-delay stated by the manufacturer.
	110 %I _s	Tripping within 0.2 s, or a time interval equal to twice the time-delay stated by the manufacturer.
	$1.05I_{r}$	No tripping within 2 h.
	$1.3I_{r}$	Tripping within 2 h.

Note: I_i - Short-circuit setting current, I_s - Overload setting current, I_r - Inverse time-delay setting current.

To generate different large testing currents, the topology we propose is illustrated in Fig. 2, in which four paralleled converting units are connected with a matrix transformer. The converter units are connected in parallel on the primary side. To supply high current, the secondary side is connected in series. C_f and L_f are designed to filter out the high frequency components. The converting units are synchronized using a CPLD-based logic control unit. To increase current accuracy, a feedforward compensator is developed based on the design of a robust adaptive estimator. The influences from the CB-dependent resistances and inductances can be effectively compensated.

A. Robust Estimator Design

The equivalent circuit for CB testing is illustrated in Fig. 3. The transfer function between testing current and port voltage can be described as follows:

$$G(s) = \frac{I(s)}{U(s)} = \frac{K}{L_l s + R_l} = \frac{K/L_l}{s + R_l/L_l} = \frac{b}{s + a}$$
 (1)

where K is the circuit gain, L_l and R_l are the equivalent inductance and resistance need to be estimated. For convenience,

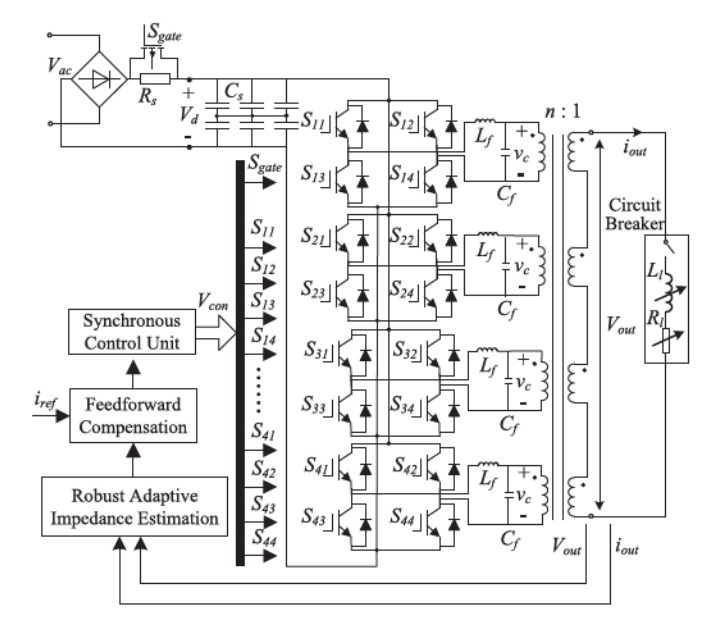


Fig. 2. Topology of the proposed system.

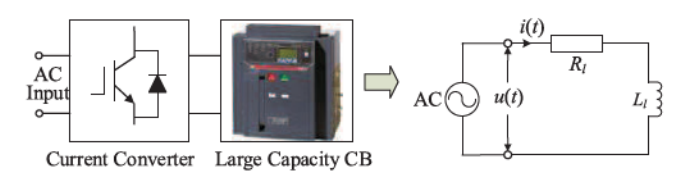


Fig. 3. Equivalent circuit of large capacity CB testing.

the transfer function is written in the Hurwitz form by defying $b = K/L_l$ and $a = R_l/L_l$.

The sI(s) term of (1) can be collected on the left side of the equation, which gives

$$sI(s) = bU(s) - aI(s). (2)$$

To avoid the derivative calculation of current in (2), the transfer function is filtered with a stable filter $\frac{1}{\chi(s)}$ and we obtain

$$\frac{s}{\chi(s)}I(s) = \frac{b}{\chi(s)}U(s) - \frac{a}{\chi(s)I(s)}$$
(3)

where $\chi(s)=s+\lambda$ and $\lambda>0$ to ensure the filter is stable. The reciprocal of λ is the time constant that determines the transient response duration. Theoretically, a smaller time constant is helpful to increase system response speed. However, this time constant cannot be too small since a very small time constant requires large calculation resources during the discretization process when the system is implemented in a hardware controller. In our design, the sampling rate is 18 kHz and λ is 9500. By defining the following notations:

$$\varphi_1^s = \frac{1}{\chi(s)} U(s), \varphi_2^s = -\frac{1}{\chi(s)I(s)}$$

$$\theta = [b, a], \quad z_s = \frac{s}{\chi(s)} I(s) = I(s) - \frac{\lambda}{\chi(s)} I(s) \quad (4)$$

the parametric model of the CB testing circuit can be described as

$$z_s = \theta \varphi_s^{\mathrm{T}} = \theta \left[\varphi_1^s, \ \varphi_2^s \right]^{\mathrm{T}}. \tag{5}$$

By solving (4) in time domain, the parametric model can be expressed as

$$z(t) = \theta \varphi^{\mathrm{T}} = \theta \left[\varphi_1(t), \, \varphi_2(t) \right]^{\mathrm{T}} \tag{6}$$

where z(t), $\varphi_1(t)$, and $\varphi_2(t)$ are the time domain solutions of z_s , φ_1^s , and φ_2^s . The parameter vector that needs to be estimated is $\theta = [b, \ a]$. Here, the gradient estimation method is used to identify the parameter vector. We assume the estimation results at time t are expressed as follows:

$$\hat{z}(t) = \hat{\boldsymbol{\theta}} \boldsymbol{\varphi}^{\mathrm{T}} \tag{7}$$

where $\hat{z}(t)$ is the estimated state and $\hat{\theta}$ denotes the parameter estimation. Combining (6) and (7), the prediction error can be expressed as

$$e(t) = \frac{z(t) - \hat{z}(t)}{m_a^2} = \frac{z(t) - \hat{\boldsymbol{\theta}}\boldsymbol{\varphi}^{\mathrm{T}}}{m_a^2} \tag{8}$$

where $m_s>0$ is the normalized factor designed to ensure that the regressor vector $\frac{\varphi}{m_s}$ is bounded. It is noted that to solve (8), the time derivative of current i(t) needs to be calculated. To avoid interference from measurement noise, a robust estimation procedure is developed based on the dead zone operator design. The objective function is defined as follows:

$$J\left(\hat{\theta}\right) = \frac{e(t)^2 m_s^2}{2} = \frac{\left(z - \hat{\theta}\varphi^{\mathrm{T}}\right)^2}{2m_s^2}.$$
 (9)

To improve the estimation robustness, the following dead zone operator is used in the parameter evolution process:

$$\dot{\hat{\boldsymbol{\theta}}} = \begin{cases} -\gamma \nabla J \left(\hat{\boldsymbol{\theta}} \right) = -\gamma \left[\frac{\partial J}{\partial \hat{\theta_1}}, \frac{\partial J}{\partial \hat{\theta_2}} \right], \ |e(t)m_s| > p_0 > \frac{|\eta|}{m_s} \\ 0, \quad \text{other} \end{cases}$$

where η represents the system disturbances and noises, p_0 is the upper bound of the disturbance error $|\eta|/m_s$, γ is the evolution factor. It is seen from (10) that the gradient evolution begins only when e(t) exceeds the designed upper bound. Otherwise the parameter vector is kept as a constant. In this way the interference from measurement noise can be filtered out. Since $\left[\frac{\partial J}{\partial \hat{q}_1}, \frac{\partial J}{\partial \hat{q}_2}\right] = -e(t)\varphi$, the gradient calculation of (10) gives the following equation:

$$\dot{\hat{\theta}} = \gamma \varphi \left(e(t) + p \right)$$

$$p = \begin{cases}
-e, & |e(t)m_s| \le p_0 \\
0, & |e(t)m_s| > p_0 > \frac{|\eta|}{m_s}
\end{cases}$$
(11)

To avoid the absolute value calculation of (11), the absolute value function can be replaced with the three segments piecewise function shown as follows:

$$\dot{\hat{\theta}} = \gamma \varphi \left(e(t) + p \right)
p = \begin{cases} \frac{p_0}{m_s}, & e(t)m_s < -p_0 \\ -\frac{p_0}{m_s}, & e(t)m_s > p_0 \\ -e(t), & -p_0 \le e(t)m_s \le p_0 \end{cases} .$$
(12)

By combing (6)–(8) and (12), the separate values of R_l and L_l can be adaptively estimated from online signals u(t) and i(t). Here, the dead zone operator has been employed in the estimation procedure, the interference from unwanted measurement noise can be filtered out.

B. Control Strategy and Dead-Time Compensation

To increase current accuracy, an adaptive feedforward compensator combined with PI control is developed to compensate the influences of CB-dependent impedance. The control strategy is illustrated in Fig. 4. By using the estimation results from (12), the CB impedance of the primary side of the transformer can be expressed as $\hat{Z}_l = n^2(\hat{R}_l + j\hat{L}_l)$, where n is the transformer ratio, \hat{R}_l and \hat{L}_l are the estimations of the CB resistance and inductance. When the inverter switching frequency is much higher than the frequency of the modulating signal $V_{\rm con}$, an averaged continuous-time model can be derived by using the KVL and KCL as follows:

$$\dot{\mathbf{X}}(t) = \begin{bmatrix} \frac{-R_f}{L_f} & 0 & \frac{-1}{L_f} \\ 0 & \frac{\hat{R}_l}{\hat{L}_l} & \frac{1}{n^2 \hat{L}_l} \\ \frac{1}{C_f} & \frac{-1}{C_f} & 0 \end{bmatrix} \mathbf{X}(t) + \begin{bmatrix} \frac{k_{\text{pwm}}}{L_f} \\ 0 \\ 0 \end{bmatrix} V_{\text{con}} \quad (13)$$

where the state variable $\mathbf{X}(t)$ is defined as $\mathbf{X}(t) = [i_i(t), i_l(t), v_c(t)]^\mathrm{T}, i_i(t)$ is the current of the filter inductor L_f , $v_c(t)$ is the voltage of the filter capacitor C_f , and $i_l(t)$ is the current of the equivalent load \hat{Z}_l . If the triangular carrier wave v_{car} is used to modulate V_{con} , the modulation index is calculated as $k_{\mathrm{pwm}} = V_d/v_{\mathrm{car}}$.

If the testing current is generated with only one converting unit, with the given reference current i_{ref} , the compensation

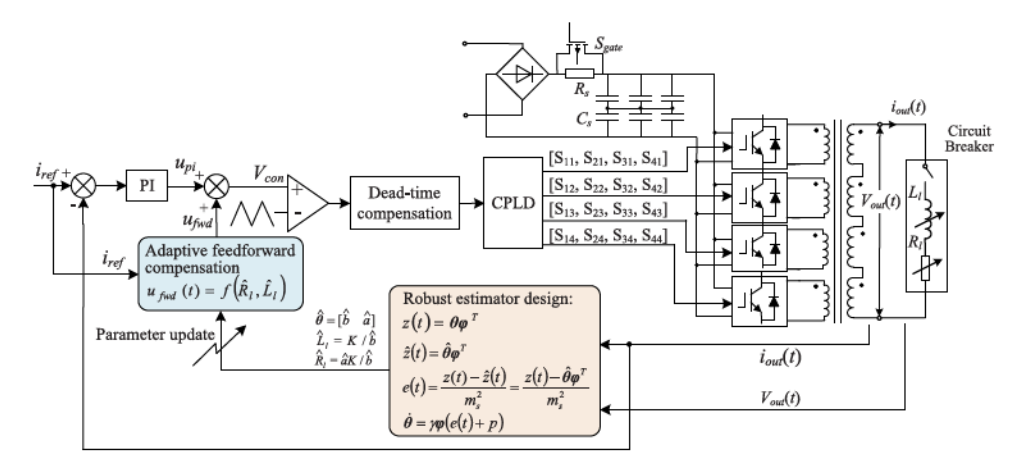


Fig. 4. Adaptive control strategy of the current converter.

voltage u_{ctl} can be obtained by solving (13)

$$u_{ctl} = n\Theta + \hat{R}_l \left(\frac{i_{ref}}{n} + nC_f \frac{d\Theta}{dt} \right) + L_f \frac{d}{dt} \left(\frac{i_{ref}}{n} + nC_f \frac{d\Theta}{dt} \right)$$
(14)

where $\Theta = i_{\text{ref}} \hat{R}_l + \hat{L}_l \frac{di_{\text{ref}}}{dt}$. It is noted that there are four converting units in our design and the primary sides of the four transformers are connected in parallel. So, the actual feedforward compensation voltage u_{fwd} applied to each unit is

$$u_{fwd} = \frac{1}{4}u_{crl}. (15)$$

From Fig. 4, it is seen that the total control voltage is the sum of PI control u_{pi} and the feedforward compensation u_{fwd} . With the given reference i_{ref} and the estimations of \hat{R}_l and \hat{L}_l , the CB-dependent impedance can be adaptively compensated.

When implementing the control voltage with the power switches in Fig. 2, the upper and lower switches in each converting bridge need to be operated in the opposite state to avoid short circuit. However, there is switching ON/OFF time for each device which could lead to conduction overlap between the upper and lower switches. To avoid this, time delay needs to be inserted when switching the devices ON and OFF. To decrease the voltage distortion caused by the inserted time delay, the controlled PWM signals are compensated by introducing a dead time compensation voltage (DTCV) along with current polarity. The value of DTCV $u_{\rm DTCV}$ corresponds to an average value of the difference between ideal and actual voltages

$$u_{\text{DTCV}} = \frac{T_c}{T_s} V_{\text{dc}} \text{sgn} \left(i_{\text{out}}(t) \right) \tag{16}$$

where T_c is the compensation time, T_s is the switching period, and $V_{\rm dc}$ is the dc-link voltage. The sign operator sgn is used in (16) to detect the current polarity. The compensated time T_c is defined as

$$T_c = T_d + t_{\rm on} - t_{\rm off} + \frac{V_{\rm on}}{V_{\rm dc}} T_s \tag{17}$$

where T_d , $t_{\rm on}$, $t_{\rm off}$, and $V_{\rm on}$ are dead time, turn-ON time, turn-OFF time, and average ON-voltage, respectively. The determination of $V_{\rm on}$ can be found in [28].

C. Simulation Results

To perform simulations, the preset values (real values) of resistance and inductance are set as $R_l=23.5~\mathrm{m}\Omega$ and $L_l=$ 0.01575 mH, and the initial guesses are taken as $R_0 = 21$ m Ω and $L_0 = 0.013$ mH, respectively. The transformer capacity in each converting unit is set as 250 kVA. Three different simulations have been conducted to verify the strategy, including Group A, Group B, and Group C. In Group A, the pure feedforward compensation is adopted. The control voltage is implemented with (15), in which the estimated parameters \hat{R}_l and \hat{L}_l are replaced with the initial guesses. In Group B, pure feedforward compensation plus with PI control are conducted, in which the proportional and integral factors are set as $k_p = 0.03$ and $k_i =$ 8000, and the resistance and inductance are based on the initial guesses. In Group C, the proposed RAF compensation plus with the PI control are adopted. The CB-dependent resistance and inductance R_l and L_l are adaptively estimated from the initial guesses $R_0=$ 21 m Ω and $L_0=$ 0.013 mH, and the PI parameters are the same as in Group B.

Before the three groups of simulations, a pure feedforward compensation is first conducted to verify (15). We first assume R_0 and L_0 are exactly the same as R_l and L_l . The magnitude of reference current is 100 A and the frequency $f_{\rm ref}$ is 50 Hz. The modulating frequency to generate the driving PWMs is 18 kHz. Simulation results are shown in Fig. 5. It is seen that the reference current can be fully tracked after a short period of transient response. The steady-state error is almost zero, which means the reference current can be fully tracked as long as the CB impedance is known. The limited steady-state error comes from the numerical approximation algorithm and the sampling frequency in the simulation. The transient error comes from the system dynamics of the testing circuit.

If the CB impedance is not known, we have conducted the three groups of simulations to demonstrate the tracking performance if the control voltage is implemented from $R_0=21~\mathrm{m}\Omega$ and $L_0=0.013~\mathrm{mH}$. Simulation results are shown in Fig. 6. It is seen in Group A that since the initial guesses deviate from the preset values, the pure feedforward compensation is not able to generate high accuracy test currents. In Group B, it is seen that

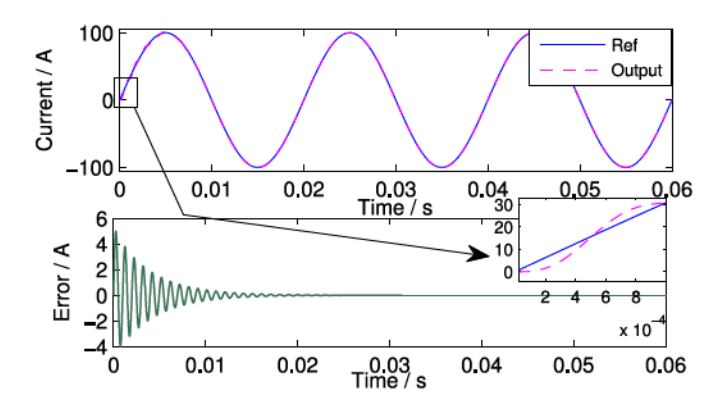


Fig. 5. Current generation if CB impedance is assumed to be known.

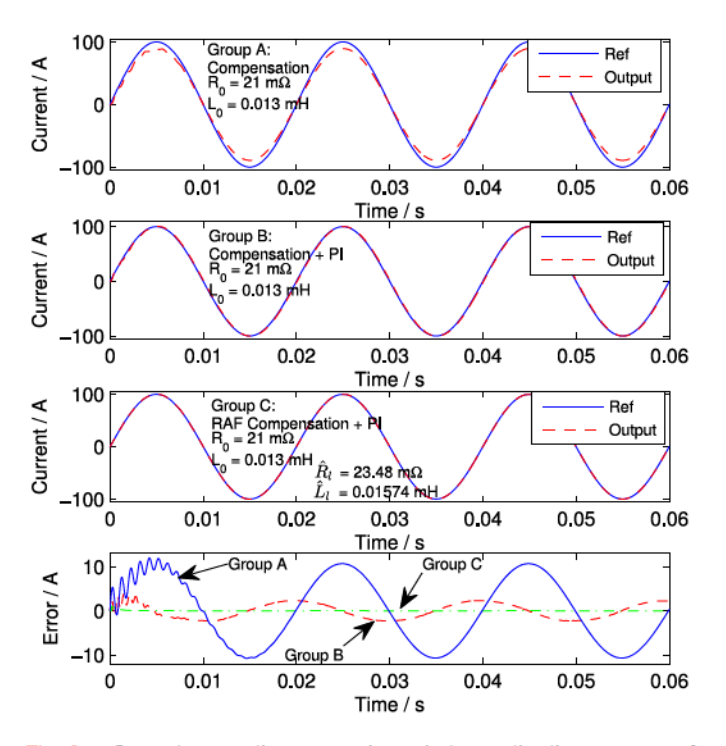
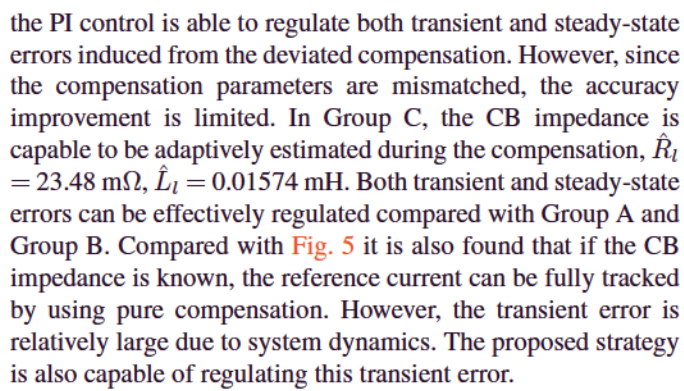


Fig. 6. Current generation comparisons between the three groups of simulations when $i_{\rm ref}=100$ A and $f_{\rm ref}=50$ Hz.



For Group C, the corresponding impedance estimations are illustrated in Fig. 7. The normalized factor is $m_s=0.2$, the evolution factors are $\gamma_1=10600$ and $\gamma_2=580700$. It is seen that starting from the initial values, both \hat{R}_l and \hat{L}_l are able to

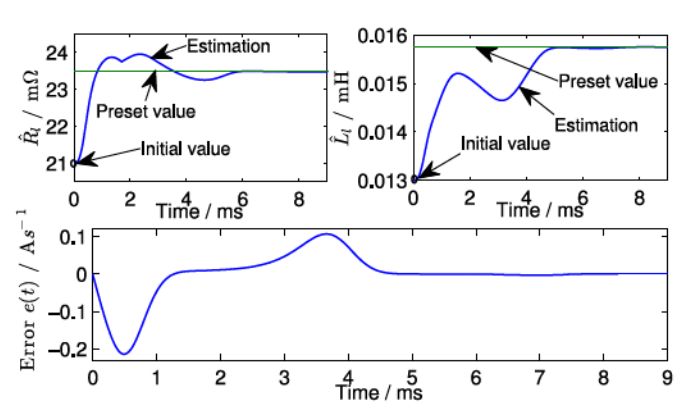


Fig. 7. Estimations of R_l and L_l when $i_{ref} = 100$ A and $f_{ref} = 50$ Hz.

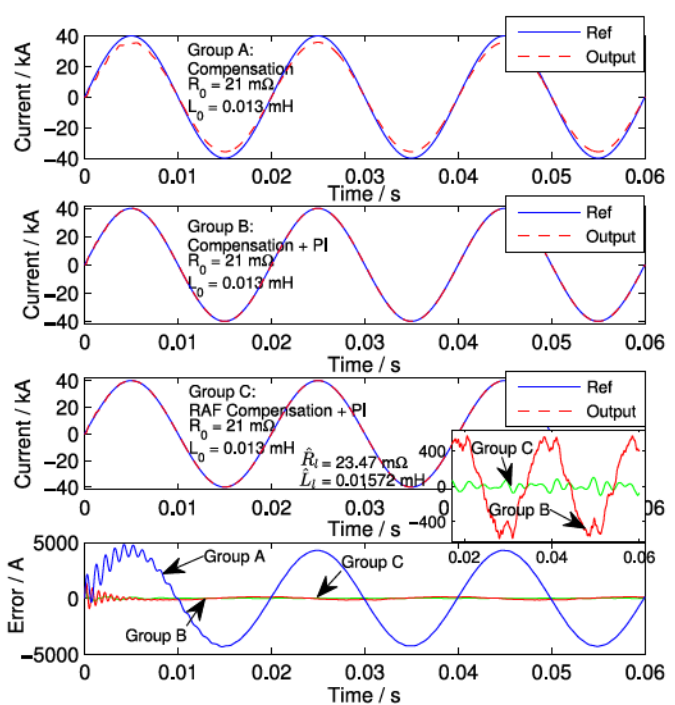


Fig. 8. Current generation comparisons between the three groups of simulations when $i_{\rm ref}=40$ kA and $f_{\rm ref}=50$ Hz (test Type I).

converge to the preset values within a short period. The convergence duration is about 6 ms, which is consistent with the transient error illustrated in Fig. 6. This comparison demonstrates that the convergence process is one of the reasons that contributes to the transient error in generating standard testing current.

The proposed converter is capable of generating a wide range of testing current from 100 A to 40 kA. There are four groups of windings in the transformer to tune the output range, 380:380, 380:127, 380:42, and 380:14. For the short-circuit test Type I shown in Table I, if the CB rated current is $I_n=3000$ A and the short-circuit setting current $I_i=7I_n$, then the testing current requires at least $I_{\rm out}=120\% I_i=25.2$ kA (RMS value). By considering the testing margin, here, we set the magnitude of the reference as $i_{\rm ref}=40$ kA. Simulation results are shown in Fig. 8. It is seen that the proposed converter is capable of

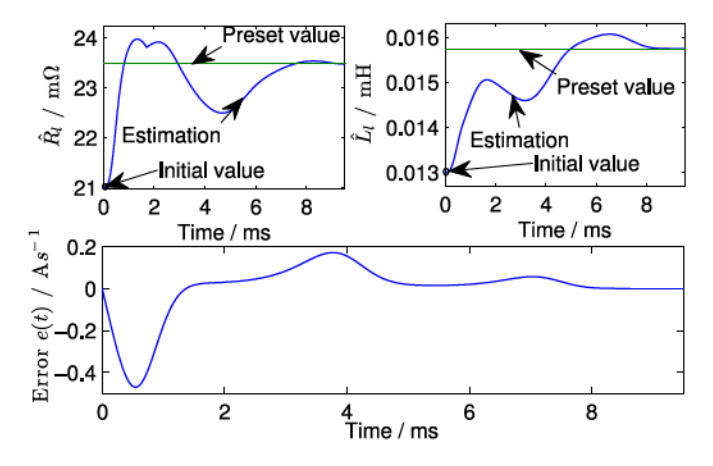


Fig. 9. Estimations of R_l and L_l when $i_{ref} = 40$ kA and $f_{ref} = 50$ Hz.

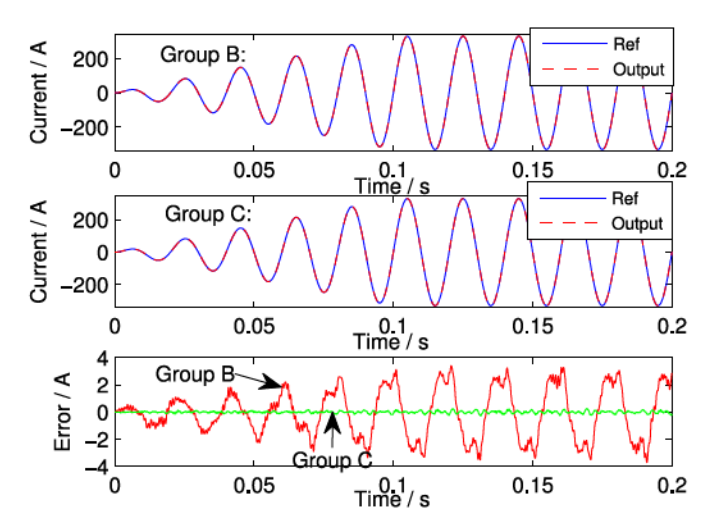


Fig. 10. Comparisons of ramped current generations for test Type II (the magnitude of i_{ref} is ramped from 0 to 313 A).

generating high precision current for large capacity CB testing with rated current up to $I_n=3000\,$ A. If I_i is set as $5I_n$, the capacity can go up to $I_n=4700\,$ A. Compared with Group A and Group B, it is seen that since R_l and L_l are adaptively estimated, both transient and steady-state errors are regulated within limited small regions for Group C. Estimations of R_l and L_l are shown in Fig. 9. Compared with Fig. 7, it is seen that the convergence trends are similar. However, the convergence duration is longer. The estimation error e(t) converges to nearly zero within 8 ms, which is larger than 6 ms in Fig. 7, and this is the reason that the transient error in Fig. 8 is larger.

For the overload test Type II, the current needs to be ramped from 0 to $1.3I_r$. Here, we assume that $I_n=200~\rm A$, $I_r=0.85I_n$. So, the testing current is $i_{\rm ref}=1.3I_r=221~\rm A$ (RMS value). Simulation results are shown in Fig. 10. From Figs. 6 and 8, it is found that pure feedforward compensation is not ideal for current regulation. Here, we only compare Group B and Group C. It is seen that while $i_{\rm ref}$ is ramped from 0 to 313 A, tracking errors in both ramped stage and steady-state stage can be regulated within limited regions for both groups. Compared with Group B, the

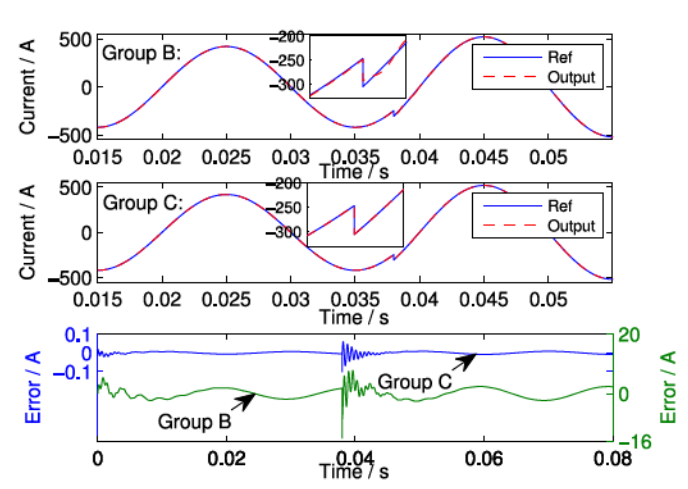


Fig. 11. Comparisons of stepped current generations for test Type II (the magnitude of $i_{\rm ref}$ is stepped from 420 A to 520 A).

error of Group C is much smaller since \hat{R}_l and \hat{L}_l are adaptively estimated. An overload protection test is implemented based on the heat accumulation principle. According to Table I, an overload test needs to last for at least 2 h. Since the accumulated heat is $W_Q = I_{\rm out}^2 R_l t$, it is seen that even small inaccuracy of current can lead to large testing errors after 2 h of accumulation and this is the reason that accuracy of testing current is critical to ensure high reliability.

According to test Type II, the " $1.05I_r$ " and " $1.3I_r$ " tests should be implemented in sequence, which means there would be a step change in current generation. Here, we assume $I_r = I_n$ and the testing current is stepped from $1.05I_r = 420\,$ A to $1.3I_r = 520\,$ A. Simulation results are shown in Fig. 11. It is required in Table I that both " $1.05I_r$ " and " $1.3I_r$ " tests need to be conducted for 2 h. To save calculation time, we set the signal step location at $0.038\,$ s and the total simulation time is $0.08\,$ s. From Fig. 11, it is seen that both transient and steady-state errors of Group C are smaller than for Group B. The error of Group C is regulated within $\pm 0.1\,$ A, whereas the maximum error of Group B exceeds $-15\,$ A. Due to the step change at $0.038\,$ s, transient errors are induced in both groups. However, the magnitude and duration of this error is much smaller in Group C.

III. EXPERIMENTAL RESULTS

The experimental setup is shown in Fig. 12, in which four paralleled converting units are connected with a matrix transformer. The controller board includes a master unit and three slave units. Synchronization is controlled with the master unit based on a CPLD circuit. The electric contactors are used to tune the transformer ratios. The transformer capacity in each converting unit is 250 kVA. The rated current and voltage of the power switches are 2 kA and 800 V. Four groups of sensors with ratios 500/5, 2000/5, 10000/5, and 40000/5 are used to obtain a wide range of current. To quantify η , we directly measure the instrument output without applying input and the values of η are 0.5, 2, 15, and 28. The value for voltage measurement is 0.5. To implement CB testing, electric motors are used to load the CB contacts with



Fig. 12. Experimental setup of testing ACB with different rated currents.

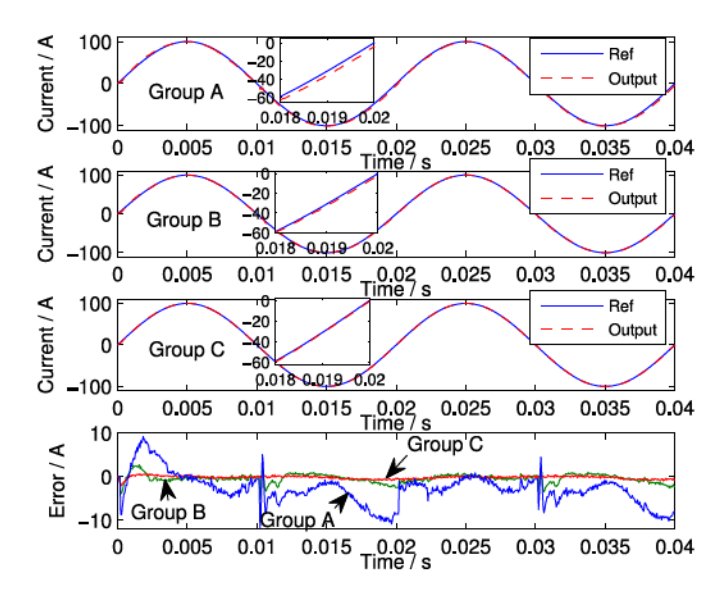


Fig. 13. Experimental comparisons of testing current generations when $i_{\rm ref}=100$ A and $f_{\rm ref}=50$ Hz.

the testing fixtures. CB testing with different capacities have been conducted to verify the proposed framework. For rated current $I_n=1000\,$ A, current generations with magnitude of 100 A are shown in Fig. 13, in which comparisons of Group A, Group B, and Group C are illustrated. It is seen that the proposed strategy Group C is able to decrease the errors. Errors of Group A are the largest and this is consistent with the simulation results.

To verify current generations with magnitude of 40 kA, we choose the CB with $I_n=3600$ A. According to the requirements of test Type I, if the testing current is $80\%I_i$ and $I_i=10I_n$, the CB is able to endure a current of 40 kA and the current waveforms are shown in Fig. 14. It is seen that the error of Group C is regulated within 2.2%, which is only 1/4 of the error in Group B. The larger error mainly comes from the mismatched impedance in compensation. The estimated \hat{R}_l and \hat{L}_l corresponding to testing currents 100 A and 40 kA are shown in Figs. 15 and 16. It is seen that in both figures \hat{R}_l and \hat{L}_l converge to steady-state values in a finite amount of time, which

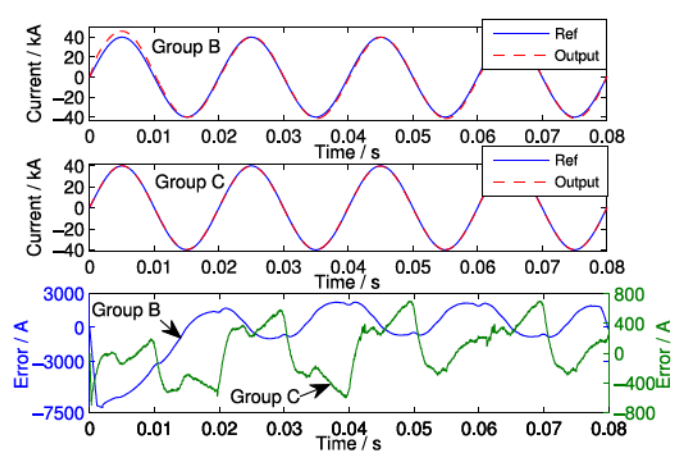


Fig. 14. Experimental comparisons of testing current generations when $i_{\rm ref}=40$ kA and $f_{\rm ref}=50$ Hz.

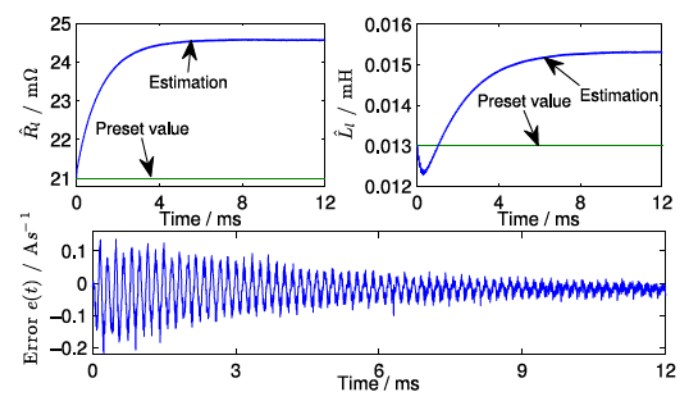


Fig. 15. Experimental results of \hat{R}_l and \hat{L}_l estimations when the magnitude of $i_{\rm ref}$ is 100 A, $f_{\rm ref}=50$ Hz and the CB capacity is $I_n=1000$ A.

means the impedance can be effectively estimated. In Fig. 15, the rated current of CB is 1000 A and the estimated \hat{R}_l and \hat{L}_l are 24.58 m Ω and 0.0154 mH. In Fig. 16, $I_n=3600$ A, \hat{R}_l and \hat{L}_l are 37.13 m Ω and 0.0352 mH, demonstrating 51% and 129% change compared with results in Fig. 15. The proposed

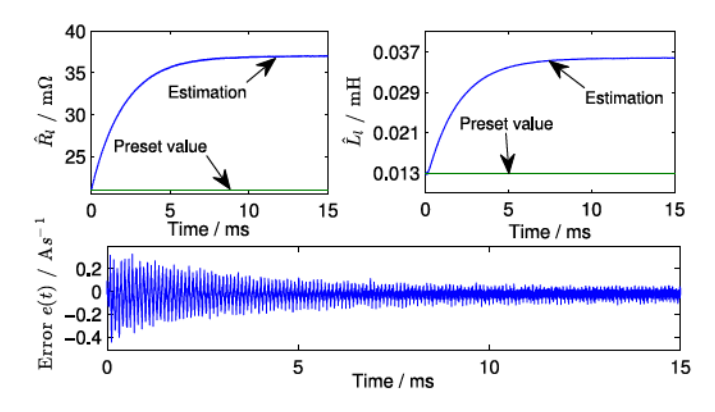


Fig. 16. Experimental results of \hat{R}_l and \hat{L}_l estimations when the magnitude of $i_{\rm ref}$ is 40 kA, $f_{\rm ref}=50$ Hz and the CB capacity is $I_n=3600$ A.

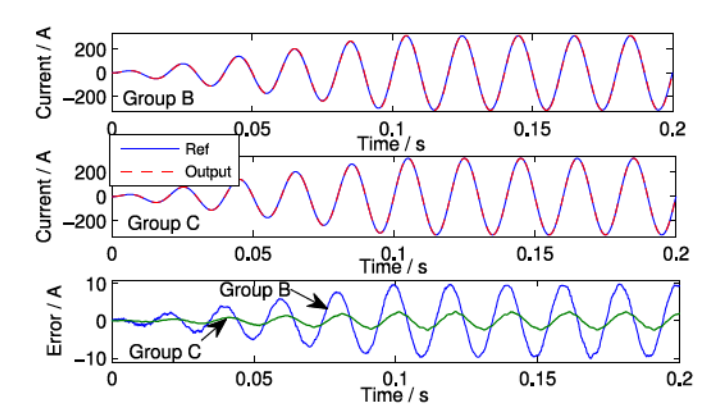


Fig. 17. Experimental comparisons of ramped current generations for test Type II (the magnitude of i_{ref} is ramped from 0 to 313 A).

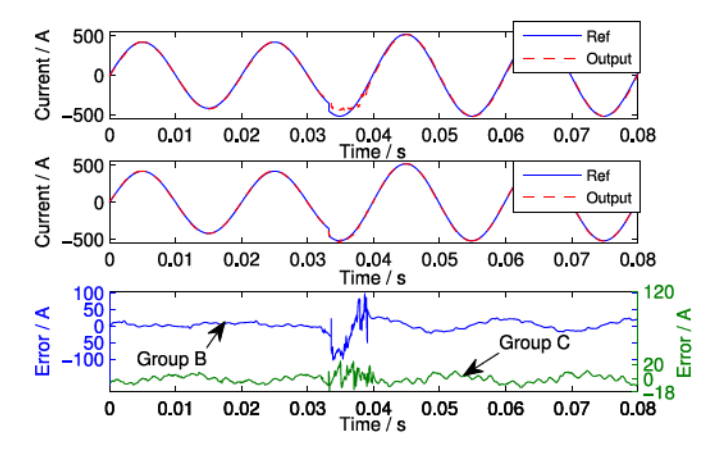


Fig. 18. Experimental comparisons of stepped current generations for test Type II (the magnitude of $i_{\rm ref}$ is stepped from 420 to 520 A).

method is capable of estimating this change and improve the testing accuracy.

To verify overload test Type II, ramped and stepped currents are generated. Here, we choose the CB with $I_n=1000$ A and the experimental results are shown in Figs. 17 and 18. It is seen that for ramped current generation, the error of Group C is regulated

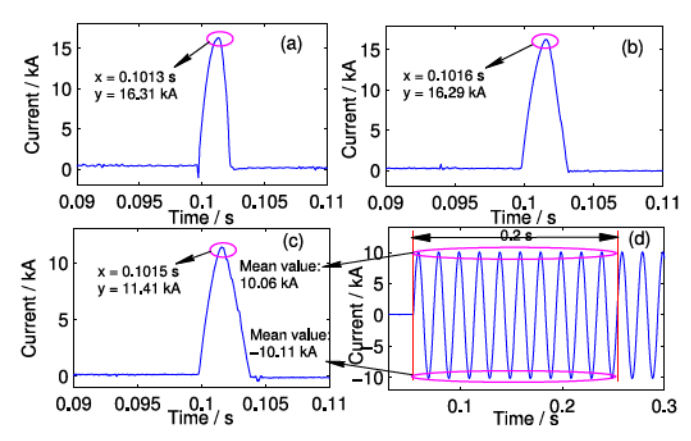


Fig. 19. Experimental verifications of breaking test Type I. (a) Group B, the $120\%I_i$ test. (b) Group C, the $120\%I_i$ test. (c) Group B, the $80\%I_i$ test. (d) Group C, the $80\%I_i$ test.

within 1%, which is nearly 1/3 of the error in Group B. From Fig. 18, it is also seen that the proposed strategy is not only able to regulate steady-state error, but also to increase the transient response speed. Current inaccuracy due to step disturbance can be effectively compensated in Group C.

Test Type I of $120\%I_i$ requires that the CB needs to break when the circuit encounters large short-circuit current. If I_n is 1000 A, $I_i = 9.5I_n$, the CB needs to break when the magnitude of short-circuit current is $\sqrt{2} \times 1.2I_i = 16119$ A. To verify the tripping test, the reference is set as 16.2 kA. Experimental results of breaking tests are shown in Fig. 19(a) and (b), in which (a) is based on Group B and (b) is based on Group C. It is seen that the CB is successfully tripped in both (a) and (b), which means the $120\%I_i$ test is satisfied. It is noted that the experiments (a) and (b) are the tripping tests and the currents at the tripping points are not the steady-state values. For the $80\%I_i$ test of test Type I, it is required that the CB has no tripping within 0.2 s when the short-circuit current magnitude is $\sqrt{2} \times 0.8I_i = 10746$ A. Here, the reference is set as 10 kA. Experimental results are shown in Fig. 19(c) and (d), in which (c) is based on current generation of Group B and (d) is based on Group C. It is seen that the CB encounters testing failure in (c). At the tripping point, the generated current of Group B is 14.1% larger than the setting value and consequently the CB is wrongly tripped at the point y = 11.41 kA. In test (d), the testing current is generated with high precision. The mean value of the magnitude is -10.11 kA and 10.06 kA. The CB has no tripping within at least 0.2 s and the testing requirement is satisfied.

IV. CONCLUSION

A matrix transformer based indirect current converter has been developed for the large-capacity CB testing application. The influences of CB-dependent contact resistances and inductances have been studied. It is found that there are at least 51% and 129% variations of equivalent resistance and inductance for CBs with different capacities. To ensure high current accuracy, a RAF control strategy has been developed to compensate for

the impedance variations. Different forms of current generation, including sinusoidal, ramp, and step, have been studied according to the IEC standards. Experimental results show that the proposed converter is able to output a wide range of current from 100 A to 40 kA, which can be used for large capacity CB testing with rated current up to $I_n=4700$ A. The proposed compensation strategy is capable to regulate both steady state and transient errors. Current errors are decreased from 6.2% to 2.2% and the CBs testing requirements of three-zone protection are fully satisfied.

REFERENCES

- S. S. Biswas, A. K. Srivastava, and D. Whitehead, "A real-time datadriven algorithm for health diagnosis and prognosis of a circuit breaker trip assembly," *IEEE Trans. Ind. Electron.*, vol. 62, no. 6, pp. 3822–3831, Jun. 2015.
- [2] C. H. Lee, B. H. Shin, and Y. B. Bang, "Designing a permanent-magnetic actuator for vacuum circuit breakers using the Taguchi method and dynamic characteristic analysis," *IEEE Trans. Ind. Electron.*, vol. 63, no. 3, pp. 1655–1664, Mar. 2016.
- [3] Circuit-Breakers for Over Current Protection for Household and Similar Installations, IEC 60898-1, Nov. 2015.
- [4] Low-Voltage Switchgear and Controlgear—Part 2: Circuit-Breakers, IEC 60947-2, Jan. 2013.
- [5] S. Kitcharoenwat, M. Konghirun, and A. Sangswang, "A novel single-phase ac-ac converter for circuit breaker testing application," *IEEE Trans. Ind. Appl.*, vol. 50, no. 6, pp. 3867–3875, Nov. 2014.
- [6] Y. J. Zhang and X. B. Ruan, "AC–AC converter with controllable phase and amplitude," *IEEE Trans. Power Electron.*, vol. 29, no. 11, pp. 6235–6244, Nov. 2014.
- [7] A. A. Khan, H. Cha, and H. F. Ahmed, "An improved single-phase direct PWM inverting buck-boost AC–AC converter," *IEEE Trans. Ind. Electron.*, vol. 63, no. 9, pp. 5384-5393, Sep. 2016.
- [8] A. Maia and C. Jacobina, "Single-phase AC-DC-AC multilevel fiveleg converter," *IET Power Electron.*, vol. 7, no. 11, pp. 2733–2742, Nov. 2014.
- [9] E. Dos Santos, N. Rocha, and C. B. Jacobina, "Suitable single-phase to three-phase AC-DC-AC power conversion system," *IEEE Trans. Power Electron.*, vol. 30, no. 2, pp. 860–870, Feb. 2015.
- [10] P. Alemi, Y. C. Jeung, and D. C. Lee, "DC-link capacitance minimization in t-type three-level AC/DC/AC PWM converters," *IEEE Trans. Ind. Electron.*, vol. 62, no. 3, pp. 1382–1391, Mar. 2015.
- [11] H. F. Ahmed, H. Cha, A. A. Khan, J. Kim, and J. Cho, "A single phase buck boost matrix converter with only six switches and without commutation problem," *IEEE Trans. Power Electron.*, vol. 32, no. 2, pp. 1232–1244, Feb. 2017.
- [12] C. F. Garcia, M. E. Rivera, J. R. Rodríguez, P. W. Wheeler, and R. S. Peña, "Predictive current control with instantaneous reactive power minimization for a four-leg indirect matrix converter," *IEEE Trans. Ind. Electron.*, vol. 64, no. 2, pp. 922–929, Feb. 2017.
- [13] J. Solanki, N. Fröhleke, J. Böcker, A Averberg, and P. Wallmeier, "High-current variable-voltage rectifiers: State-of-the-art topologies," *IET Power Electron.*, vol. 8, no. 6, pp. 1068–1080, Jun. 2015.
- [14] H. Li et al., "Thermal coupling analysis in a multichip paralleled IGBT module for a DFIG wind turbine power converter," IEEE Trans. Energy Convers., vol. 32, no. 1, pp. 80–90, Mar. 2017.
- [15] D. Bortis, J. Biela, and J. W. Kolar, "Active gate control for current balancing of parallel-connected IGBT modules in solid-state modulators," *IEEE Trans. Plasma Sci.*, vol. 36, no. 5, pp. 2632–2637, Oct. 2008.
- [16] B. M. Ge, X. Lu, X. H. Yu, M. S. Zhang, and F. Z. Peng, "Multiphase-leg coupling current balancer for parallel operation of multiple MW power modules," *IEEE Trans. Ind. Electron.*, vol. 61, no. 3, pp. 1147–1157, Mar. 2014.
- [17] B. M. Ge and F. Z. Peng, "Current balancer-based grid-connected parallel inverters for high power wind-power system," *Int. Trans. Elect. Energy*, vol. 24, no. 1, pp. 108-124, Jan. 2014.
- [18] T. H. Ding, J. Wang, H. F. Ding, L. Li, B. H. Liu, and Y. Pan, "A 35 kA disc-shaped thyristor DC switch for batteries power supply of flat-top pulsed magnetic field," *IEEE Trans. Appl. Supercond.*, vol. 22, no. 3, Jun. 2012, Art. no. 5400404.

- [19] C. Klosinski et al., "Hybrid circuit breaker-based fault detection and interruption in 380 V dc test-setup," in Proc. Annu. Holm Conf. Elect. Contacts, Jul. 2018, vol. 2018, pp. 203–210.
- [20] J. K. Pradhan, A. Ghosh, and C. N. Bhende, "Small-signal modeling and multivariable PI control design of VSC-HVDC transmission link," *Electric Power Syst. Res.*, vol. 144, pp. 115–126, Mar. 2017.
- [21] V. Monteiro, J. C. Ferreira, A. A. N. Melendez, and J. L. Afonso, "Model predictive control applied to an improved five-level bidirectional converter," *IEEE Trans. Ind. Electron.*, vol. 63, no. 9, pp. 5879–5890, Sep. 2016.
- [22] I. Yazici and E. K. Yaylaci, "Fast and robust voltage control of dc-dc boost converter by using fast terminal sliding mode controller," *IET Power Electron.*, vol. 9, no. 1, pp. 120–125, Jan. 2016.
- [23] H. C. Chen and J. Y. Liao, "Modified interleaved current sensorless control for three-level boost PFC converter with considering voltage imbalance and zero-crossing current distortion," *IEEE Trans. Ind. Electron.*, vol. 62, no. 11, pp. 6896–6904, Nov. 2015.
- [24] U. Jakobsen, K. Lu, P. O. Rasmussen, D. H. Lee, and J. W. Ahn, "Sensorless control of low-cost single-phase hybrid switched reluctance motor drive," *IEEE Trans. Ind. Appl.*, vol. 51, no. 3, pp. 2381–2387, May 2015.
- [25] L. Shu, M. Dapino, G. C. Wu, and D. F. Chen, "Frequency-dependent sliding-mode control of Galfenol-driven unimorph actuator based on finiteelement model," *IEEE Trans. Ind. Electron.*, vol. 63, no. 2, pp. 1071–1082, Feb. 2016.
- [26] F. J. Azcondo, A. de Castro, V. M. Lopez, and O. Garcia, "Power factor correction without current sensor based on digital current rebuilding," *IEEE Trans. Power Electron.*, vol. 25, no. 6, pp. 1527–1536, Jan. 2010.
- [27] H. C. Chen and J. Y. Liao, "Design and implementation of sensorless capacitor voltage balancing control for three-level boosting PFC," *IEEE Trans. Power Electron.*, vol. 29, no. 7, pp. 3808–3817, Jul. 2014.
- [28] N. Urasaki, T. Senjyu, K. Uezato, and T. Funabashi, "An adaptive deantime compensation strategy for voltage source inverter fed motor drives," *IEEE Trans. Power Electron.*, vol. 20, no. 5, pp. 1150–1160, Sep. 2005.



Liang Shu (Member, IEEE) received the B.S. degree in electrical engineering and automation from China Three Gorges University, Yichang, China, in 2005, and the M.S. and Ph.D. degrees in mechanical engineering from the Wuhan University of Technology, Wuhan, China, in 2008 and 2011, respectively.

From September 2008 to January 2011, he was a Research Assistant in mechanical engineering with The Ohio State University, Columbus, OH, USA. Since 2011, he has been with

Wenzhou University, Wenzhou, China, where he is currently a Professor of Electrical and Electronic Engineering College. His research interests include intelligent electrical apparatus, mechatronics, and dynamic control.

Prof. Shu is a Senior Member of Chinese Mechanical Engineering Society, and he is also a Senior Committee Member of the Robot Branch of Chinese Mechanical Engineering Society. He is currently the Associated Director for the Low Voltage Apparatus Technology Research Center of Zhejiang, China. He also serves as the Associated Director for the Technology Institute of Wenzhou University, Yueqing, China.



Ziran Wu received the B.S. degree in information engineering from Zhejiang University, Hangzhou, , China, in 2007, and the M.Sc. and Ph.D. degrees in electronic engineering from the University of York, York, U.K., in 2008 and 2013, respectively.

Since 2014, he has been with Wenzhou University, Wenzhou, China, where he is currently an Associate Professor of the Electrical and Electronic Engineering College. His research interests include artificial intelligence, smart man-

ufacturing, and machine vision.

Dr. Wu is the Associated Director of the Technology Institute of Wenzhou University, Yueqing, China, and he is also the Associated Director of the Zhejiang Technology Service Platform of Wenzhou Low-voltage Apparatus.



Yingmin You received the B.S. degree in applied physics from Fuzhou University, Fuzhou, China, in 2002, and the M.Sc. degree in instrument science and technology from Chongqing University, Chongqing, China, in 2009. He is currently working toward the Ph.D. degree in electrical engineering with the School of Electrical Engineering, Hebei University of Technology, Tianjin, China.

From July 2002 to August 2006, he was a Research Lecturer with the Department of Physics

and Electronic Engineering, Minnan Normal University, Fujian, China. Since 2009, he has been with Wenzhou University, Wenzhou, China, where he is currently an Engineer of the Electrical and Electronic Engineering College. His research interests include power electronics, system reliability analysis and control.



Sheng Zhao received the B.S. and M.S. degrees in instrument measurement and control technology from the Hefei University of Technology, Hefei, China, in 2001 and 2005, respectively, and the Ph.D. degree in electrical engineering from the Hebei University of Technology, Tianjin, China, in 2015.

Since 2005, he has been with Wenzhou University, Wenzhou, China, where he is currently an Associate Professor of the Electrical and Electronic Engineering College. His research in-

terests include power electronics and intelligent control.



Marcelo J. Dapino received the Engineering Diploma in mechanical and industrial engineering from the University of Uruguay, Montevideo, Uruguay, in 1994, and the Ph.D. degree in engineering mechanics from Iowa State University, Ames, IA, USA, in 1999.

He is the Honda R&D Americas Designated Chair in Engineering at The Ohio State University, Columbus, OH, USA, where he is a Professor with the Department of Mechanical and Aerospace Engineering. He serves as the

Director of the Smart Vehicle Concepts Center (a National Science Foundation Industry-University Cooperative Research Center), and is a Senior Fellow of The Ohio State University Center for Automotive Research. His research interests are design and manufacture of smart material systems.

Prof. Dapino is a Fellow of the American Society of Mechanical Engineers (ASME) and the International Society for Optics and Photonics (SPIE).